International Journal for Multidisciplinary Research (IJFMR)
E-ISSN: 2582-2160 ● Website: www.ijfmr.com ● Email: editor@ijfmr.com

Land Surface Temperature and Urban Heat Island: A Case Study of Faridabad City using RS and GIS techniques

Abhishek Malik[1], Gaurav Kalotra[2]

[1]Research Scholar: Panjab University, Chandigarh
[2]Professor: Panjab University, Chandigarh

Abstract
Land use and land surface temperature both plays a crucial role in the global climate change studies, as a little fluctuation in these, can bring about a dramatic impact on the regional as well as global environment. With rapid urbanization many regions across the world are altering the existing land use/land cover (LULC), which is significantly raising the land surface temperature (LST). The present study aims to estimate the land use change and land surface temperature and what changes does both bring about in a span of 20 years over Faridabad MC. Faridabad being a part of Delhi NCR has seen rapid growth of population in last two decades which has severely impacted its Land cover. Landsat imagery of 2002, 2013 and 2022 has been used for estimating both the LULC and LST of the city. Supervised classification with Maximum likelihood Classification (MLC) which is basically a machine learning based algorithm has been adopted for LULC classification and Mono window algorithm has been used for the retrieval of LST. UTFVI (Urban Thermal Field Variance Index) has also been calculated which showed different Urban heat islands across the city. The results reveal a rapid increase in the built-up area and reduction in the vegetation and agricultural land. Similarly, Land surface temperature was highest in highly dense built-up areas as well in the barren area of Faridabad, compared to this LST was comparatively lower over the agriculture and vegetation and least of water bodies. There were several UHI hotspots over the city area, mostly located in the densely populated and industrial parts of city.

Keywords: LULC, MLC, LST, UTFVI, UHI

Introduction

Climate change is considered to show one of the most treacherous environmental impacts on ecosystem services, on environmental sustainability and on daily life. Land use/land cover change (LULC) exacerbates climate change by reducing biodiversity and increasing the urban heat island effect (UHI) in cities by increasing the land surface temperature. LULC and LST changes are considered one of the most common study topics for remote sensing scholars. In the last few decades, global urbanization has played a major role in environmental, socio-economic and demographic change. As a result of urbanisation, LULC categories such as green cover, wetlands and water bodies, as well as open fields, are undergoing rapid transformation. LULC and LST change can be used to assess the ecological health and viability of cities. An environmental phenomenon known as urban heat island (UHI) is one of the main causes of climate change. The phenomenon known as the urban heat island has spread to many parts of the world.

An urban heat island is a city or area where the temperature is significantly higher than the surrounding area (N. Li, S. Miao, 2020; Y. Wang, 2021). Another interpretation of the urban heat island is that urban areas have higher temperatures than the surrounding countryside is mainly related to the heat capacity of materials. Latent heat flux is low due to increased surface water flux increase in anthropogenic heat corresponds to the decrease of free and green spaces in urban contexts. In China, LULC changes are one of the most widespread study topics for researchers working in the field of remote sensing (Faisal (2021), Siddique (2022). Uncontrolled rapid urban growth and LULC changes can alter the hydrologic, thermodynamic and radiative processes of the Earth surface, amplifying the impacts of climate variability and heat waves. The unmonitored change of LULC also expands built up areas by removing green cover, leading to environmental degradation through UHI effects (luck and wu, 2002). Rapid urbanization increases impervious layers such as buildings, roads and factories, leading to massive increases in local surface tension (LST). These increases in LST also affect UHI phenomena and have a significant impact on biodiversity's primary function as well as local and regional climatic conditions (luck and wu, 2002). Built-up areas have higher UHI concentrations because they have additional impervious surfaces. UHI is a critical issue from the point of view of environmental development, as it has various negative consequences for urban residents (Kafy et al., 2020c). UHI concepts are addressed by LST estimation based on freely available, easily accessible remote sensors with higher spatiotemporal resolution (Kafy et al., 2020a). In particular, historical medium-resolution Landsat data are repeatedly used to determine LST and characterize the UHI effect (Choudhury et al., and 2019; Kafy et al., 2021).

First, Rao in year 1972, mentioned the Surface Urban Heat Island (SUHI) effect using a remote sensing satellite. Remote sensing data were used in UHI or LST studies obtained from various satellite sensors. Many previous studies have demonstrated the importance of thermal infrared (TIR) data due to their accessibility at various spatial and temporal resolutions (Aniello et al. 1995; Streutker 2003; Voogt and Oke 2003; Chen et al. 2006; Tran et al. 2006; Tiangco et al. 2008; Zhang et al. 2010). The intensity of the UHI depends on different factors such as the difference in the composition of the LULC between urban and rural areas, the thermal conductivity of urban surfaces, the vegetation cover in cities, human emissions derived from human activities and housing density (Taha 1997 ; Sarrat et al. 2006; Mathew et al. 2016; Zhang e Wang 2008)..

Due to the variations in spatial LULC, the pattern of spatial landscapes is changing in many rural regions, and therefore it has become critical to detect LULC changes at an appropriate scale with accurate time series data. Knowledge of its relationship with climate change in urban areas then emerges, helping to understand various environmental impacts (Almazroui et al., 2013; Siddique et al., 2020). Many mathematical indices have been used by researchers worldwide to help them better understand LULC changes (Mishra and Prasad, 2015). The most commonly used index is the Normalized Difference Vegetation Index (NDVI), which describes the vegetation condition using a combination of the red and near-infrared bands of satellite images (Gascon et al., 2016).

However, although LULC and LST results are easy to visualize with available Landsat records, predicting future changes is a difficult task. Markov Chain (MC), Cellular Automata (CA) and Artificial Neural Network (ANN) models are used to predict LULC changes (Balzter, 2000; Zenil, 2010). MC models are considered when LULC change is well known but spatially dependent and cannot be promoted (Kafy et al., 2020b; Ullah et al., 2019). Climate change in urban environments is stimulating research on UHI, and strategies can be developed to reduce the negative effects of UHI on climate. India is the second largest country and is a major factor in increasing urbanization. Hence, there is an urgent need to study SUHI

growth and urban growth in Indian cities. The intensity of the UHI depends on the urban LST and the rural land cover surrounding the cities. Most of the rural land cover is vegetation or barren land, both of which have different thermal patterns during daylight hours, which influence the determination of UHI intensity. Several previous studies have discussed the combination of impervious soil and buildings to form UHI. Since urbanization is the result of the replacement of arid or vegetated land by buildings, it is important to study the impact of buildings on the structure of the UHI.

Faridabad, the industrial capital of Haryana, has experienced rapid urban growth due to significant urban development and rural-urban migration. Growing population pressure has accelerated unplanned expansion in the region. Methods such as CA-ANN algorithms can be useful in identifying the short and long-term dimensions of LULC and LST transformations in this region. It can also help decision makers and urban planners to reduce the UHI phenomenon. Thus, this study analyzes the chronological change of LULC and its effect on LST, investigates the relationship of LST between different LULC classes, and performs a correlation analysis of different land cover indices with LST during the years 2002, 2013, and 2022. This study used Maximum likelihood image classification for LULC and mono window algorithms for the LST retrieval and based on that UHI and UTFVI has been calculated.

Objective of the Study

There are 2 objectives for the current study

- To know the land use and land cover and Land Surface Temperature of Faridabad City from year 2002 to 2022.
- To examine the Urban Heat Islands and Urban Thermal Field Variance Index over the Faridabad city.

Study area

The study is based in Faridabad city with latitude range 28° 16° 59°N - 28° 30° 26°N and longitude range 77° 22° 3°E - 77° 20° 21°E. Faridabad is the largest city in Haryana, India (Census of India) and is part of the National Assembly of Delhi. It is one of the satellite cities around Delhi and is located 284 km south of Chandigarh city. The Yamuna River is the eastern boundary of Uttar Pradesh and the region. On 24 May 2016, the Government of India included it in the second phase of the Smart Cities Mission. Faridabad is the ninth fastest growing city in the world and the third fastest growing city in India, according to the City Mayors Foundation report. Faridabad is included in the National Capital Region of Delhi under the Delhi Regional Plan (DMA), 2001 (Town and Country Planning Organisation, 2007).

According to the 2011 Census of India, the total urban population of Faridabad is 14,38,855, Faridabad MC is 14,14,050, which is 98.27% of the urban population of Faridabad district. Faridabad city has a growth rate of 36.26% and a literacy rate of 84.88%. There are 872 women for every 1,000 men. Major cities and major industries are well connected to the city by road, rail and metro.

The Delhi-Agra National Highway 44 runs through the city and its heart. It has one main railway station, Faridabad (FDB), two smaller railway stations on the Northern Railway division of Indian Railways and a metro line that runs from Ballabgarh on the Delhi-Mathura highway. Faridabad is also known as the industrial capital of Haryana. In 2013, of the 11,665 registered factories in Haryana, 2,499 were located in Faridabad, which increased to 2,886 in 2019 (Statistical Abstract of Haryana, 2019).

The area is developing as a small city in itself with wide roads, tall buildings, shopping malls, educational institutions, medical facilities and shopping malls. Zones 66 to 74 are industrial and zones 75 to 89 are residential (Acme Spaces, 2015). The World Health Organization (WHO) ranked Faridabad as the second

most polluted city in the world in 2018. Faridabad ranks 10th among the 10 dirtiest cities in India in 2020 according to the Swachh Surekha Survey (Swachh Survekshan 2020).

Fig 1: Study area Map

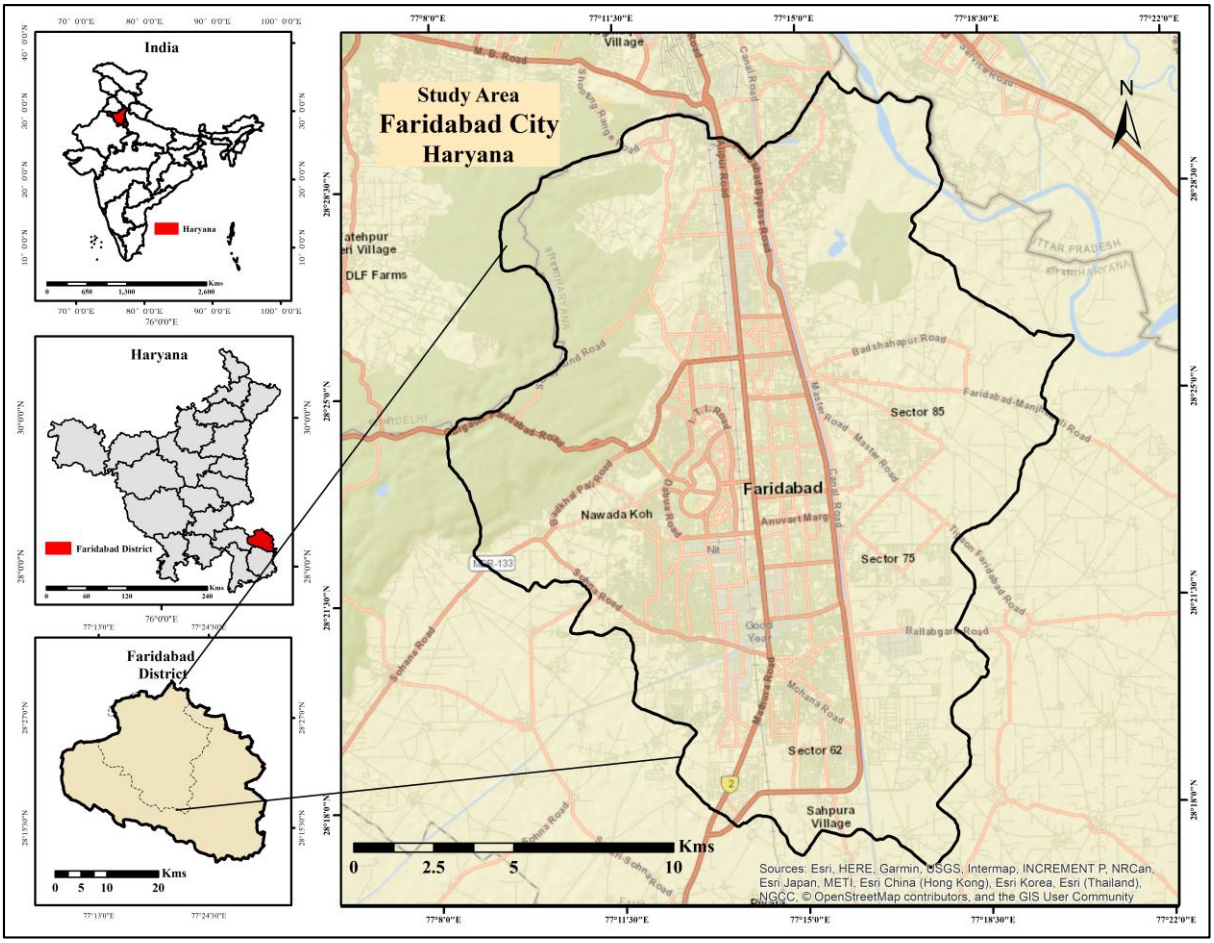

Source: 1. Shapefile from: *Faridabad Metropolitan Development Authority* ***(FMDA) Onemap Portal.***
2. Basemap from: *ESRI, HERE, Garmin, USGS.*

Methodology

The methodological flow chart shows a brief steps followed during study

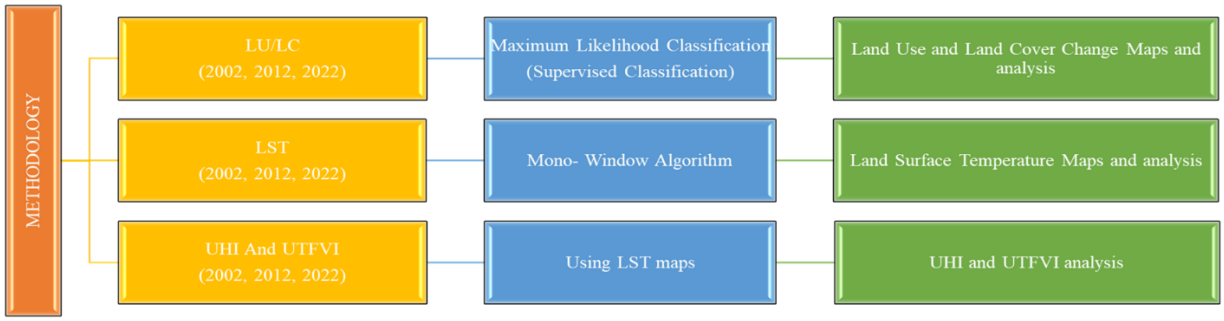

1. Data acquisition information

Multispectral Landsat data from the USGS Earth Explorer were taken to monitor LULC changes, LST distribution, and different indices such as UHI and UTFVI. The images were taken from the same month

to avoid the effects of seasonal changes as they are less than 10%. However, all Landsat features in the study area are cloud-free. Landsat images were not ground corrected, image-to-image correction and geometric distortion were performed (Kafy et al., 2020b). **Table 1** provides detailed information on the data obtained.

Sensor	Sensor	Date	Path/ Row	Bands Used
Landsat 7	ETM+	08-06-2002	146/40	B1,B2,B3,B4,B5,B6
Landsat 8	OLI/ TIRS	29-05-2013	146/40	B2,B3,B4,B5,B6,B7,B10
Landsat 8	OLI/TIRS	22-05-2022	146/40	B2,B3,B4,B5,B6,B7,B10

Table 1. Downloaded Landsat satellite images information from USGS.

3. LULC classification

For LULC classification, different steps such as image preprocessing was done by performing radiometric and atmospheric correction using ERDAS Imagine V14 software. After the corrections, images were classified into five major classes: Agriculture, barren land (open land) vegetation cover, built-up areas, water bodies for 2002, 2013 and 2022. A suitable colour combination was used to classify the LULC classes using approximate 50 training samples. The Maximum likelihood Classification (MLC) algorithm, a non-parametric classifier and was used to classify the LULC classes. National Remote Sensing Centre (NRSC) developed Land Cover Classification System (LCCS) that provides an effective framework for LULC classification, and in this study, the guideline provided by NRSC is followed (NRSC, 2018).

After the classification was done, the classified LULC map's accuracy assessment was carried out with 350 points obtained using the Google Earth pro platform and the global positioning system (GPS). All of the points were collected from Google Earth pro platforms for years 2002 and 2013, where 250 points were collected from Google Earth pro and 100 points were collected using GPS for 2022. Finally, overall classification accuracy, kappa statistics, user and producer accuracy were estimated, which is considered one of the most effective accuracy assessment approaches (Rahman et al., 2018).

4. LULC change estimation

Estimating changes in LULC classes in different years is important to determine the most important land cover factors that help reduce cool areas, such as plant cover and water. To estimate the impact of urban expansion on different LULC classes, we used the matrix integration tool of Erdas Imagin V15 software on LULC maps from 2002 to 2013, 2013 to 2022, and 2002 to 2022. We identified changing pixels in vegetation and water cover body from barren area classes to built-up areas. Matrix input checks and creates new files for the two-input (raster) project file. The generated file contains the class values that specify how the original file should be compared to the LULC class values.

5. Estimation of LST

1. **Radiation Correction:** The step includes the conversion of pixel DN (Digital Number) to at-sensor radiance, subtraction of atmospheric illumination effects and sensor calibration. While comparing multiple imageries it is better to use spectral radiance rather than using DN values directly. The

conversion is carried out with the following formula (Landsat Project Science Office, 2002, K.V. Suryabhagavan).

For **Landsat 7 ETM+**

$$\mathbf{L\lambda} = \frac{(\boldsymbol{LMax - LMin})}{(\boldsymbol{QcalMax - QcalMin})} * (\boldsymbol{Qcal - QcalMax}) + \boldsymbol{LMin}$$

where,

Lλ is the spectral radiance at sensors aperture

LMax is spectral at the Sensor Radiance scaled to QCal Max,

LMin is Spectral at the Sensor Radiance scaled to QCal Min,

QCal Max is the maximum quantized calibrated pixel values corresponding to LMax,

QCal, Min is the minimum quantized calibrated pixel value (DN) corresponding to LMin and

QCal is the quantized calibration pixel value (B. Tafesse, K.V. Suryabhagavan, 2019)

It has been proved that radiation correction improves the accuracy of LST and other index calculation (Song et al., 2001).

2. **LST Generation (Convert Radiance to BT):** The spectral radiance converted from pixel DN values is then used to compute brightness temperature (i.e., blackbody temperature) under the assumption of unit emissivity and using pre-launch calibration constants (A.S.M. Abdul Athick, K. Shankar, 2019, Landsat Project Science Office, 2002).

$$\mathbf{TB = K2 / \ln(1+(K1/L\lambda))} \qquad \text{..... (2)}$$

Where,

TB = effective temperature in Kelvin

K1 and K2 = pre-launch calibration constants

For **TM, K1** = 607.76 & K2 =1260.56

3. **Conversion of degree Kalvin to degree Celsius**: Finally, the Kelvin temperature is converted to land surface temperature in Celsius (TS) as,

$$\mathbf{TS = TB - 273} \qquad \text{.....(3)}$$

Retrieval of LST from level-1 Landsat 8 TIRS band

The retrieval method used in the study will be the Mono-Window Algorithm. The LST Mono Window (MWA) retrieval algorithms basically, depends upon linearization of Planck's radiance function. Qin et al. (2001) developed MW algorithm for retrieving LST from band 6 of Landsat 5 (TM) using three parameters namely, emissivity, transmittance and mean atmospheric temperature. Wang et al. (2015) calibrated the MW algorithm for Landsat 8 (TIRS) band 10 also. The following methodology will be implemented while retrieval of LST from Landsat 8:

a) **Initially, Conversion of DN values to radiance values**: the digital numbers (i.e. DN values) in the thermal infrared band (band 10) are converted to at-sensor radiance values.
b) Second step would be the, calculation of **Top of atmosphere (TOA)** brightness temperature which is calculated from at-sensor radiance values.
c) Third step would include, the estimation of **Land surface emissivity (LSE)** which is estimated at each pixel.
d) Final step would include, the **LST retrieval** using the **TOA brightness** temperature **and land surface emissivity**.

a) **Conversion of DN values to radiance values:**

$$\boldsymbol{L}\text{sensor} = ML * DN + AL \quad \text{(1)}$$

where,

Lsensor= At-sensor radiance (W/m2 /sr /µm).

ML = Multiplicative scaling factor: ML = 0.0537 for band 6 and ML = 0.0033 for band 10 (Source: Metadata file from Landsat 8).

AL= Additive scaling factor: AL = 1.1824 for band 6 and AL = 0.10 for band 10 (Source: Metadata file from Landsat 8).

DN= Digital number (DN value).

Estimation of TOA brightness temperature from at-sensor radiance values

$$T_B = K2 \ln (K1 \, L\text{sensor} + 1) \quad \text{(2)}$$

T_B = TOA Brightness temperature (Kelvin).

*L*sensor= At-sensor radiance (W/m2 /sr /µm).

K1 = Thermal constant 1: K1 = 607.76 for band 6 and K1 = 774.8853 for band 10 (Source: Metadata file from Landsat 8).

K2 = Thermal constant 2: K2 = 1260.56 for band 6 and K2 = 1321.0789 for band 10 (Source: Metadata file from Landsat 8).

b) Estimation of Land Surface Emissivity (LSE) using NDVI Threshold (NDVITHM) algorithm

$$\varepsilon_i = \begin{cases} \varepsilon_{s\lambda i}, & NDVI < NDVI_s \\ \varepsilon_{s\lambda i} P_v + \varepsilon_{s\lambda i}(1 - P_v) + C_{\lambda i}, & NDVI_s \leq NDVI \leq NDVI_v \\ \varepsilon_{s\lambda i} P_v + C_{\lambda i} & NDVI > NDVI_v \end{cases}$$

The LSE was estimated using NDVITHM algorithm. The algorithm uses NDVI threshold values to distinguish between soil pixels (NDVI< 0.2) and vegetation cover (NDVI> 0.5) and the emissivity values are calculated as follows (Yu et al. 2014; Sobrino et al. 2008; Griend and Owe, 1993),

(3)

Where,

a) ***Pred*** is reflectivity in the red band.

b) ***εV*** and ***εS*** are emissivity of vegetation and soil respectively. Values of εV = 0.9863 and εS = 0.9668 will be used based on Yu et al. (2014).

c) ***PV*** is the proportion of the vegetation as defined in Equation 4

$$PV = \left[\frac{NDVI - NDVI_{min}}{NDVI_{max} - NDVI_{min}}\right]^2 \quad \text{(4)}$$

where,

$NDVI_{max}$ = 0.5 and

$NDVI_{min}$= 0.2

$$\mathbf{C} = (1 - \varepsilon S)(1 - PV) F\varepsilon V \quad \text{(5)}$$

The term **C** takes the cavity effect into account due to surface roughness. Sobrino et al. (2004), suggested that C can be estimated as follows,

Where, **F** is a geometrical factor ranging from 0-1, depending on geometrical distribution of surface. A mean value of F = 0.55 (Yu et al. 2014).

The MW algorithm converts the LST using Landsat 8 TIRS band 10 through the parameter calculation, including the mean atmospheric temperature, brightness temperature, atmospheric transmittance, and land surface emissivity, as Equations. (Wang, F.; Qin, Z.; Song, C.; Tu, L.; Karnieli, A.; Zhao, S.) According to the suggestion from USGS, Landsat 8 band 10 is more accurate than band 11 and, therefore, the data of band 10 are utilized in the Mono window algorithm which only need one infrared band to convert the LST (Wang, F.; Qin, Z.; Song, C.; Tu, L.; Karnieli, A.; Zhao, S.).

$$LST = [a * (1 - C - D) + (b * (1 - C - D) + C + D) TB - D * Ta] / C \quad \text{.....(6)}$$

$$C = \tau * \varepsilon \quad \text{.....(7)}$$

$$Di = (1 - \tau)[1 + (1 - \varepsilon)\tau] \quad \text{.....(8)}$$

Where,

Ts is the **LST (K);** a* and b* are constants (Rozenstein, O.; Qin, Z.; Derimian, Y.; Karnieli, A.).

C and **D** are the parameters of band

TB is the brightness temperature (K) of band 10;

τ is the atmospheric transmittance, τ was calculated using Table;

Table: Estimation of atmospheric transmittance for band 10 (Source: Yang J and Qui, 1996; Li J, 2006**)**

Atmospheres	Water vapour content (w) (g/cm^2)	Atmospheric transmittance (τ)
Mid-latitude summer	0. 2-1.6	τ = 0.9184-0.0725 w
	1.6-4.4	τ = 1.0163–0.1330 w
	4.4-5.4	τ = 0.7029–0.0620 w
Tropical model	0.2-2.0	τ = 0.9220–0.0780 w
	2.0-5.6	τ = 1.0222–0.1310 w
	5.6-6.8	τ = 0.5422–0.0440 w
Mid-latitude winter	0.2-1.4	τ = 0.9228–0.0735 w

ε is the land surface emissivity.

The water vapour content (w) required in Table for calculation of atmospheric transmittance will bw estimated using equation (Yang J and Qui, 1996; Li J, 2006).

$$w = 0.0981 * \left\{10 * 0.6108 * \exp\left[\frac{17.27 * T_o - 273.15}{237.3 * T_o - 273.15}\right] * RH\right\} + 0.1697 \quad \text{..... (9)}$$

where, w = water vapour content (g/cm2)

To = near surface air temperature (Kelvin).

RH = relative humidity in %.

To and RH values on date of satellite pass will be provided by India Meteorological department.

Ta = effective mean atmospheric temperature (Kelvin). **Ta** will be determined using Table.

Ta = 17.9769 + 0.91715 T_0 (Table) will be used to compute Ta, as the study area is located in the Tropical area.

T_0 is near surface air temperature (Kelvin) which was provided by India Meteorological department.

Table: Effective mean atmospheric temperature (Ta) for four standard atmospheres (Source: Qin et al. 2001).

Standard atmosphere	Effective mean atmospheric temperature (T_a) (Kelvin)
For USA 1976	$T_a = 25.9396 + 0.88045\ T_0$
For tropical	$T_a = 17.9769 + 0.91715\ T_0$
For mid-latitude summer	$T_a = 16.0110 + 0.92621\ T_0$
For mid-latitude winter	$T_a = 19.2704 + 0.91118\ T_0$

Estimation of UHI and UTFVI

The Urban heat island was retrieved using the following formula. (Rahman, M. N; Rony, M. R. H; Jannat 2021)

Formula for UHI = (LST – LST_{mean}) / SD

The UTFVI index is used to measure the effect of urban heat intensity quantitatively on urban surfaces. UTFVI will be used to measure UHI in the study which will be measured using the equation below (Liu, L.; Zhang, Y.)

UTFVI = $Ts - T_{mean}/T_s$

Where,

UTFVI stands for the urban thermal field variance index,

T_s stands for the LST of a certain point(pixel) in the area, and;

T_{mean} stands for mean LST temperature of the whole study area.

UTFVI is further separated into six levels in accordance with six different ecological evaluation indexes to better depict changes (Zhang, Y.; Yu, T.; Gu, X.).

Table2: Showing Urban Thermal Field Variance Thresholds. The green colour shows the excellent condition and worst condition in red. (Liu, L.; Zhang, Y. 2011)

Urban Thermal Field Variance Index Threshold	Urban Heat Island Phenomenon	Ecological Conditions Evaluation
<0	None	Excellent
0.000-0.005	Weak	Good
0.005-0.010	Middle	Normal
0.010-0.015	Strong	Bad
0.015-0.020	Stronger	Worse
>0.020	Strongest	Worst

Above table shows the specific thresholds for each of the six UTFVI levels, where a higher urban UTFVI value shows the greater urban heat intensity and the worse condition of the ecological ecosystem by red colour. (Nautiyal, Maithani and Sharma, 2021; Maithani, Nautiyal and Sharma, 2020; Guha et al. 2017, 2018; Zhang, 2006). On the opposite side green colour shows the good condition and low UHII. The UTFVI maps will also provide the environmental quality of city which in result deliver a better understanding and information for urban land cover studies and planners.

Relationship between LULC and LST

The spatial and temporal analysis and monitoring of LST distribution on different LULC was done using the "combine" feature from "spatial analyst" toolset in ArcGIS 10.4.1 software to determine the impact of

LULC change on LST. The visible and thermal SWIR bands are used for LULC classification and LST estimation, and all images are transformed to a spatial resolution of 30 m × 30 m using a pre-relation calibration method. "unify" A toolchain that produces unique pixel values for each individual set of input values. Multiple raster matrices. The join function supports joining a given integer pixel value with an associated attribute table. If the value contains a decimal point, it is automatically truncated in the attribute table like any other entry. The output of the built-in tool summarizes the LST distributions of the LULC types and presents the characteristics as a table, showing different raster.

Result and discussion

LULC change analysis

After accessing the data, it has been seen that built-up area in the study area has seen a drastic change from 59.21 sq.km. in year 2002 to 114.45 sq.km. in year 2022 which is from 20.55% in year 2002 to 39.41% of total land in Faridabad City. Contrary to the built-up expansion it has been seen that there is dramatic change in the category of Agriculture where it has reduced to 86.64 sq.km in 2022 from 111.45 sq.km in year 2002. It has been seen that most of the built-up expansion took place over the agricultural land in the Faridabad city. (Conversion of Agricultural land to Built-up area). Area under Barren land seen a reduction as most of the area also been converted to built-up and agricultural land. Area under Vegetation has seen a little increase from 43.01 sq.km in year 2002 to 47.03 sq.km in year 2022 and Water bodies remain more over constant. After performing the accuracy assessment the results showed 83.45% accuracy for year 2002, 87.54% for year 2013 and for year 2022 it was 88.12%.

Fig 2: Map showing LULC Classification for year 2002, 2013, 2022

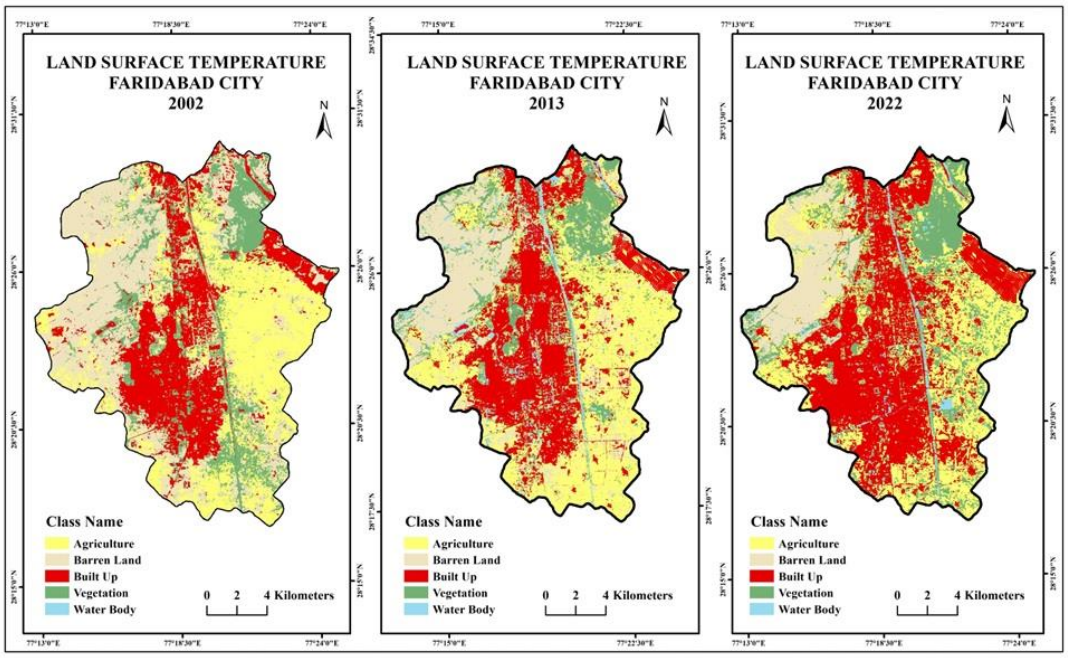

Table 3: showing results from LULC Classification (2002, 2013, 2022)

LAND USE LAND COVER CHANGE						
Year/Category	**2002 (sq.km)**	**%**	**2013 (sq.km)**	**%**	**2022 (sq.km)**	**%**
Built Up	59.21	20.55	77.21	26.68	114.45	39.61
Water Body	9.93	3.45	9.71	3.36	9.56	3.31
Agriculture	111.45	38.68	98.12	33.91	86.64	29.98

Vegetation	43.01	14.93	45.14	15.60	47.03	16.28
Barren Land	64.53	22.40	59.19	20.45	31.27	10.82
Total	288 sq.km* (Approx)					

*Data based on the results from LU/LC classification

The two most clear changing trends, can be seen here that is, increase in built-up area and decreases in barren land and land under agriculture, are distinctly noticed (table 3). From 2002 to 20222, the built-up area increased from 20.55% in year 2002, to 39.61% in year 2022. A massive decrease in barren and agriculture land were noticed. Many factors contribute to these changes, including rural-to-urban migration, unplanned infrastructure development, and unplanned urban expansion to accommodate urban population growth. The main premise found that this massive urban expansion involves strategic and economic factors that result in the scarcity of natural resources and fresh Land Covers such as tree cover and water bodies (Fu and Weng, 2018).

Fig 3: Satellite view showing a drastic change in Faridabad City over the spam of 10 years

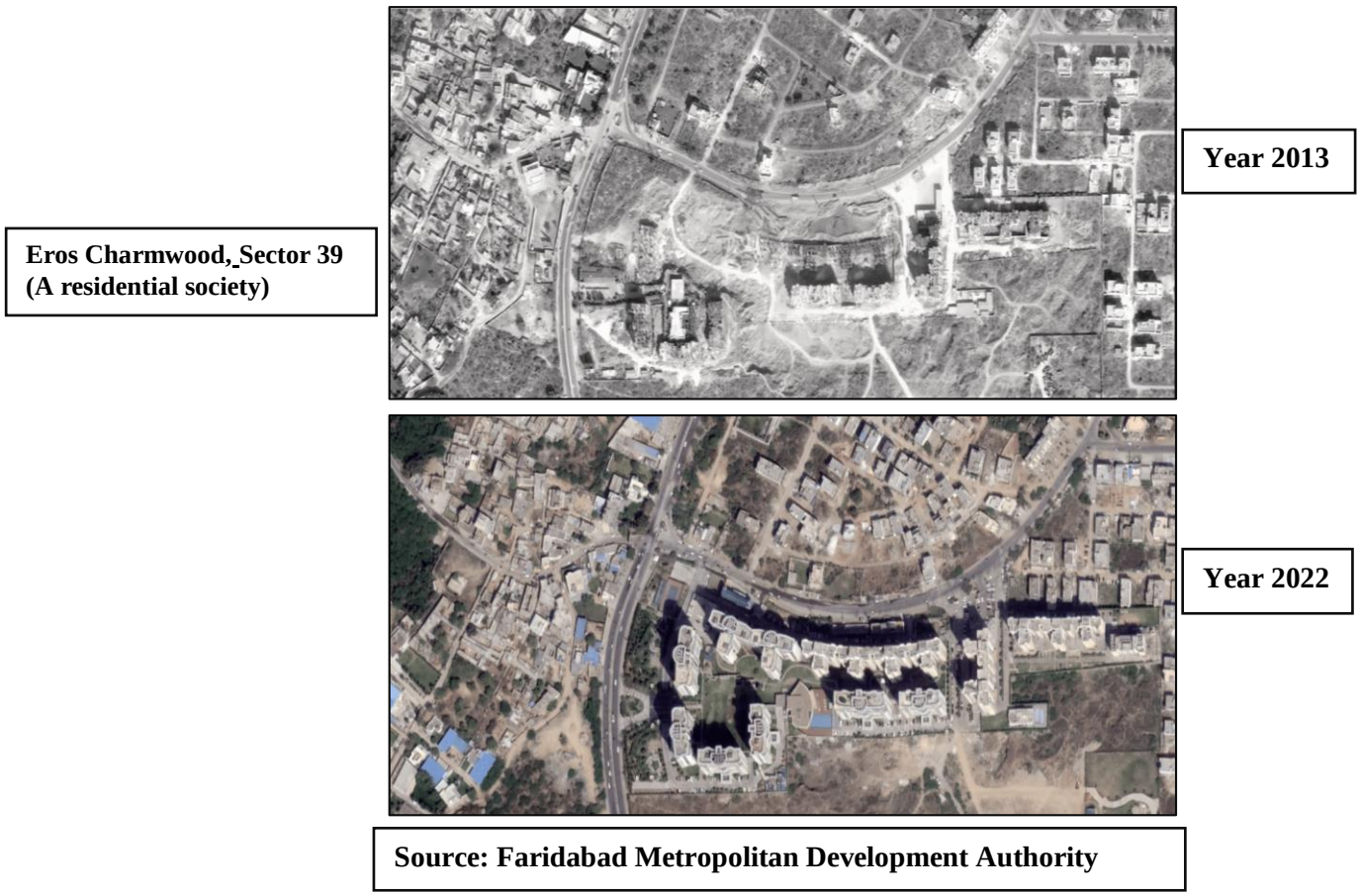

Table 4: Showing change in different intervals (2002 – 2013, 2013 – 2022, 2002 – 2022)

Year/Category	2002	2013	Change	2013	2022	Change	2002	2022	Change
Built Up	59.21	77.21	18.00	77.21	114.45	37.24	59.21	114.45	55.24
Water Body	9.93	9.71	-0.22	9.71	9.56	-0.15	9.93	9.56	-0.37
Agriculture	111.45	98.12	-13.33	98.12	86.64	-11.48	111.45	86.64	-24.81
Vegetation	43.01	45.14	2.14	45.14	47.03	1.89	43.01	47.03	4.03

Barren Land	64.53	59.19	-5.34	59.19	31.27	-27.92	64.53	31.27	-33.26

*Data in sq.km *Data based on the results from LU/LC classification

Maximum Change was seen in the **Built-up Category** which is **55.24 sq.km** after a negative change of **33.26 sq.km** was seen in **Barren Land category**, Land under **Agriculture** also seen a massive negative change of **24.81 sq.km** apart from that **Vegetation** has seen a increase of **4.03 sq.km**. Statistic, financial, and social variables all have an impact on this gigantic urban development (Weng, 2001). The design of LULC is incredibly impacted by the development and decay of the human populace. Furthermore, relocation, rural-urban populace dissemination, and urbanization all have an impact on it. Financial approaches such as arrive subsidization, cost changes and charges too impact the decision-making process of human creatures and lead to changes in designs of arrive utilize. States of mind, devout convictions, history, values, and person recognition all contribute to arrive utilize designs. The environmental results are too subordinate on the information of arrive supervisors, political and financial approaches, and administration abilities.

Variations of LST changes over the study area

1. Validation of estimated LST

The LST was determined for each of the study periods using thermal sensors in the acquired data. However, although the equation used by researchers around the world to find LST has many limitations. For the accuracy of the LST estimation process, the sky should be clear with a0(0) % cloud cover. The cloud cover of the acquired dataset may have hampered the LST estimation process producing biased results. In addition, not all surface elements have a unique emissivity value at a specific location (Neteler, 2010). These factors may cause error values in the LST distribution in the study area.

Fig 4: Showing LST map for different time period (2002, 2013, 2022)

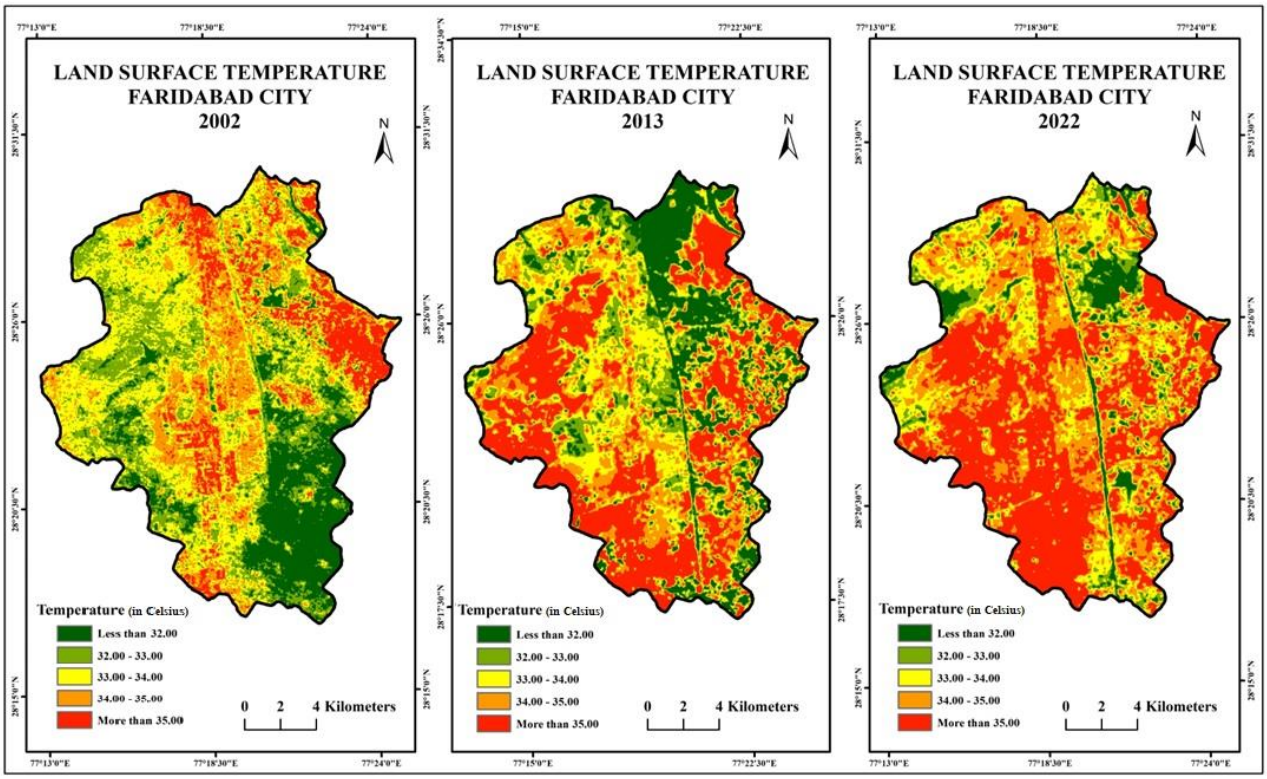

Table 5: Showing LST results

Land Surface Temperature			
Temperature (Degree Celsius)	**2002**	**2013**	**2022**
MIN	23.86	26.36	29.11
MAX	37.92	39.04	43.47
MEAN	29.67	31.87	33.54
SD	1.64	1.67	1.49

For year **2002** it was seen that the minimum LST recorded was 23.86ºC and maximum was 37.92ºC while mean was 26.67ºC with standard deviation of 1.64ºC. Similarly, for year **2013** it was seen that the minimum LST recorded was 26.36ºC and maximum was 39.04ºC while mean was 31.87ºC with standard deviation of 1.67ºC. For year **2022**, it was seen that the minimum LST recorded was 29.11ºC and maximum was 43.47ºC while mean was 33.54ºC with standard deviation of 1.49ºC. Although Remote sensing based estimated LST values have limitations influenced by global conditions, small differences between estimated and measured LST can be accepted and used for analysis in this study, such as prediction of LST.

2. Variations of LST changes over different LULC

Estimated mean LST distribution in different LULC classes for 2002, 2013, and 2022 were calculated in ArcGIS 10.4.1 software with the zonal statistics tool.

Fig 5 : Showing LULC and LST for year 2002

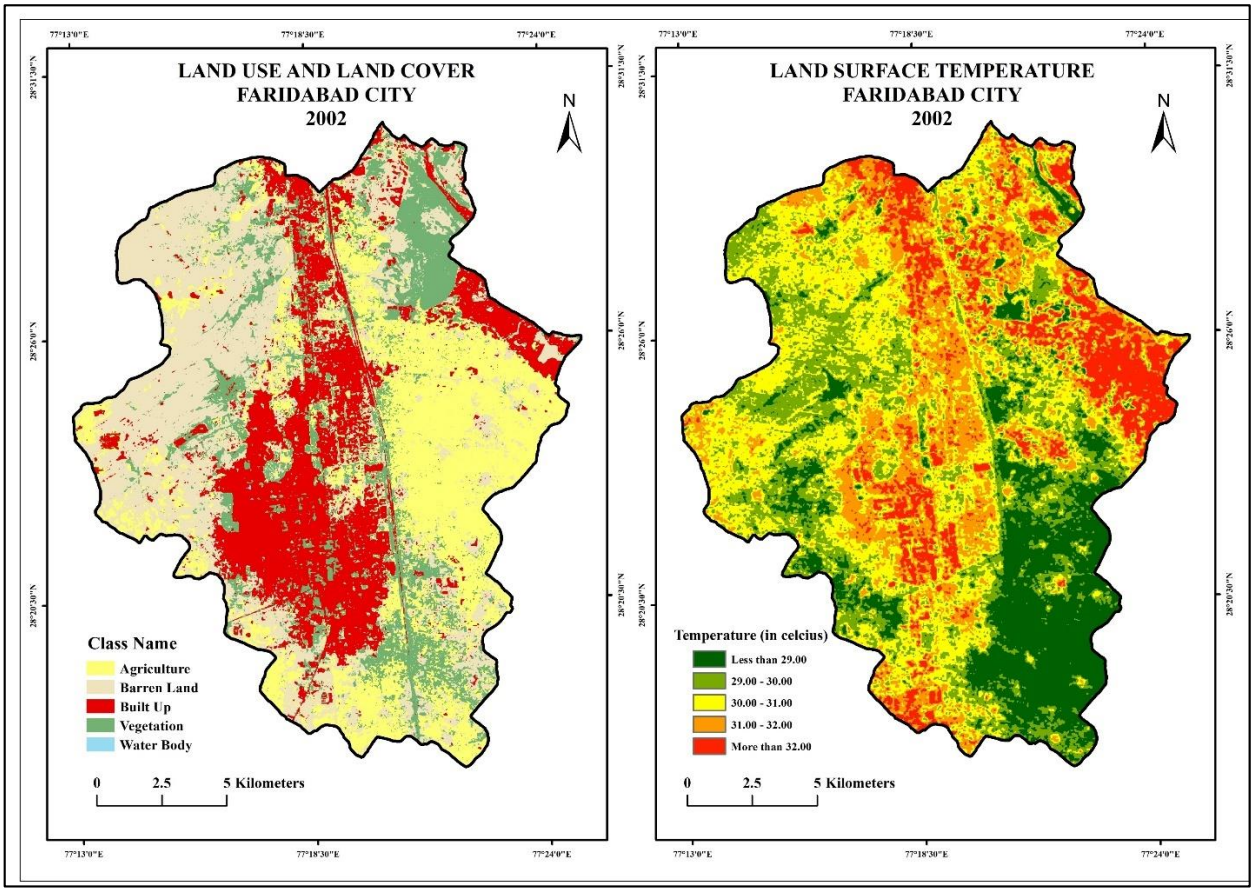

Fig 6 : Showing LULC and LST for year 2013

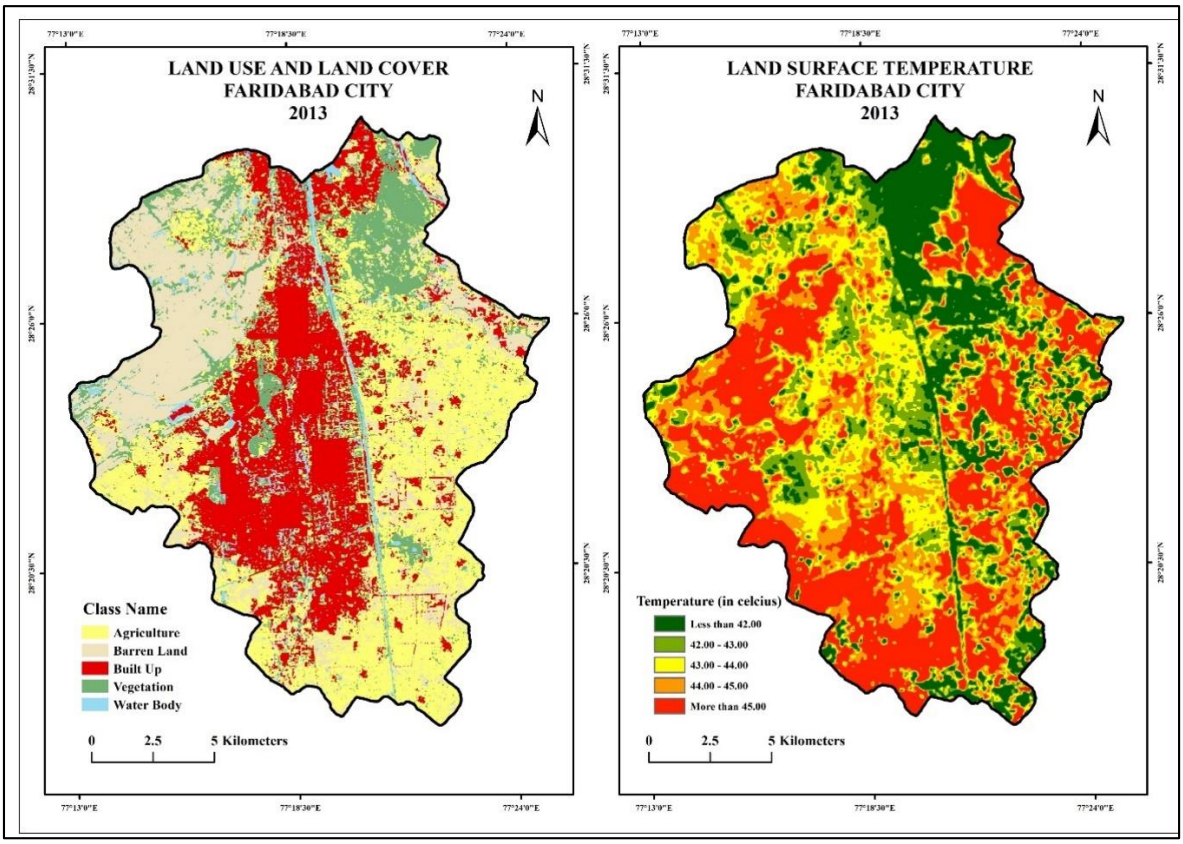

Fig 7 : Showing LULC and LST for year 2022

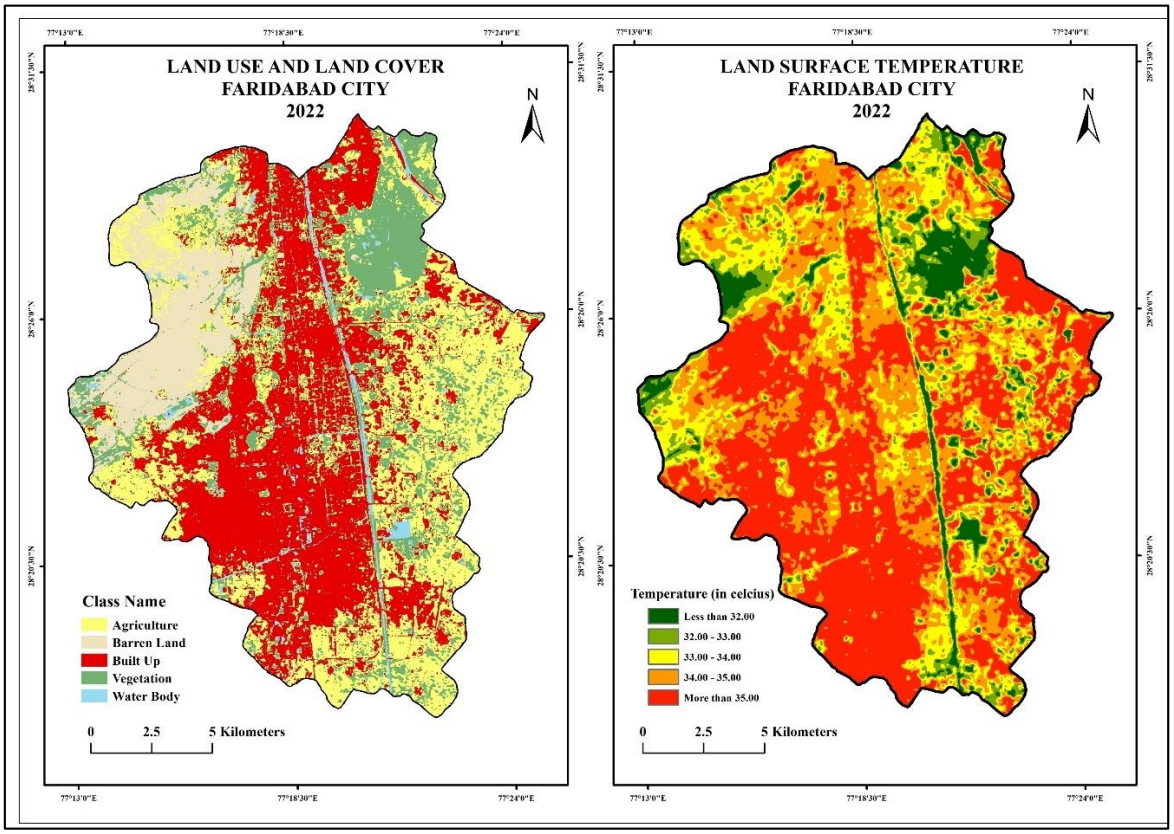

Table 6 : Showing Category wise LST values

CATEGORY	TEMPERATURE (degree c)	2002	2013	2022
AGRICULTURE	MIN	26.86	32.67	29.62
	MAX	35.92	43.03	41.79
	MEAN	30.18	37.95	34.87
	SD	1.47	1.28	1.46
BARREN LAND	MIN	27.35	34.31	29.20
	MAX	36.46	48.35	39.64
	MEAN	30.31	43.58	34.43
	SD	1.05	1.71	1.33
BUILT UP	MIN	23.86	31.86	29.41
	MAX	37.92	37.92	43.47
	MEAN	31.24	31.63	35.26
	SD	1.14	1.58	1.34
VEGETATION	MIN	24.36	31.33	27.91
	MAX	34.06	37.14	39.82
	MEAN	29.68	32.49	32.92
	SD	1.09	1.38	1.49
WATER BODIES	MIN	23.86	26.36	28.11
	MAX	32.65	33.14	34.55
	MEAN	27.84	30.55	29.90
	SD	0.9	1.8	1.18

Agriculture: In year 2002 the minimum and maximum land surface temperature recorded was 26.86ºC and 35ºC and mean temperature recorded was 30.18ºC with a Standard Deviation of 1.47. Similarly in year 2013 the min and max temperature recorded was 32.67ºC and 43.03ºC with mean temp of 37.95ºC and SD of 1.28. and for year 2022 the min and max temp recorded was 29.62ºC and 41.79ºC with mean of 34.87ºC and SD of 1.46ºC.

Barren Land: In year 2002 the minimum and maximum land surface temperature recorded was 27.35ºC and 36.46ºC and mean temperature recorded was 30.31ºC with a Standard Deviation of 1.05. Similarly in year 2013 the min and max temperature recorded was 34.31ºC and 48.35ºC with mean temp of 43.58ºC and SD of 1.71. and for year 2022 the min and max temp recorded was 29.20ºC and 39.64ºC with mean of 34.43ºC and SD of 1.33ºC.

Built-up: In year 2002 the minimum and maximum land surface temperature recorded was 26.36ºC and 37.92ºC and mean temperature recorded was 31.24ºC with a Standard Deviation of 1.14. Similarly in year 2013 the min and max temperature recorded was 31.59ºC and 37.04ºC with mean temp of 31.63ºC and SD of 1.58. and for year 2022 the min and max temp recorded was 29.41ºC and 43.47ºC with mean of 35.26ºC and SD of 1.34ºC.

Vegetation: In year 2002 the minimum and maximum land surface temperature recorded was 24.36ºC and 34.06ºC and mean temperature recorded was 29.68ºC with a Standard Deviation of 1.09. Similarly in year 2013 the min and max temperature recorded was 31.33ºC and 37.14ºC with mean temp of 32.649ºC and SD of 1.38. and for year 2022 the min and max temp recorded was 27.91ºC and 39.92ºC with mean of 32.92ºC and SD of 1.49ºC.

Water Bodies: In year 2002 the minimum and maximum land surface temperature recorded was 23.86ºC and 32.65ºC and mean temperature recorded was 27.68ºC with a Standard Deviation of .09. Similarly in year 2013 the min and max temperature recorded was 28.36ºC and 33.14ºC with mean temp of 30.55ºC and SD of 1.8. and for year 2022 the min and max temp recorded was 28.11ºC and 34.55ºC with mean of 29.90ºC and SD of 1.18ºC.

Results of UHI and UTFVI

The UHI findings shows that the built-up area showed the maximum levels of temperatures. Results ranges from 4.24 degree Celsius (in year 2002) to 5.34 degree Celsius (in year 2022), which show that there is a increase of at least 1 degree Celsius temperature over the Built-up Category. Vegetation and Water bodies show a inverse impact of UHI with least effect or with no UHI forming. Barren land also show positive values for UHI due to the absorption of heat.

Fig 8 : Showing UHI map for year 2002

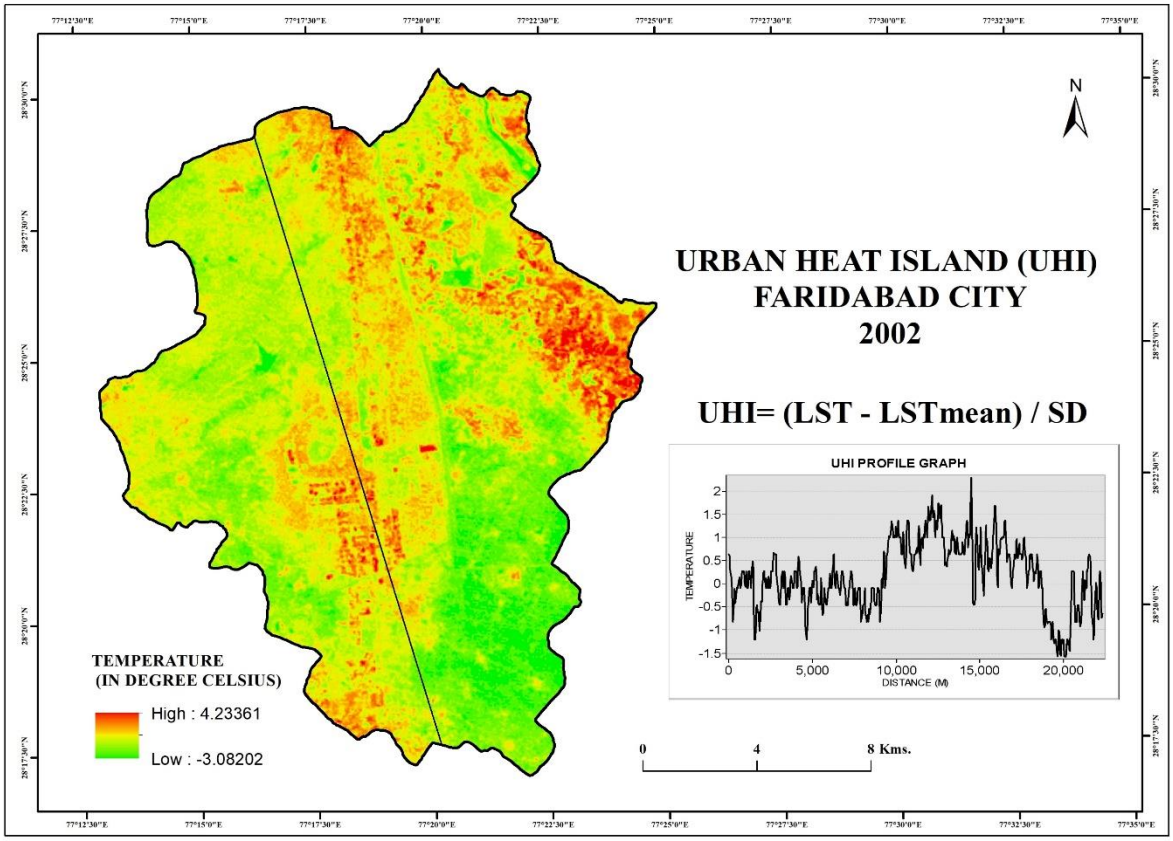

Fig 9 : Showing UHI map for year 2013

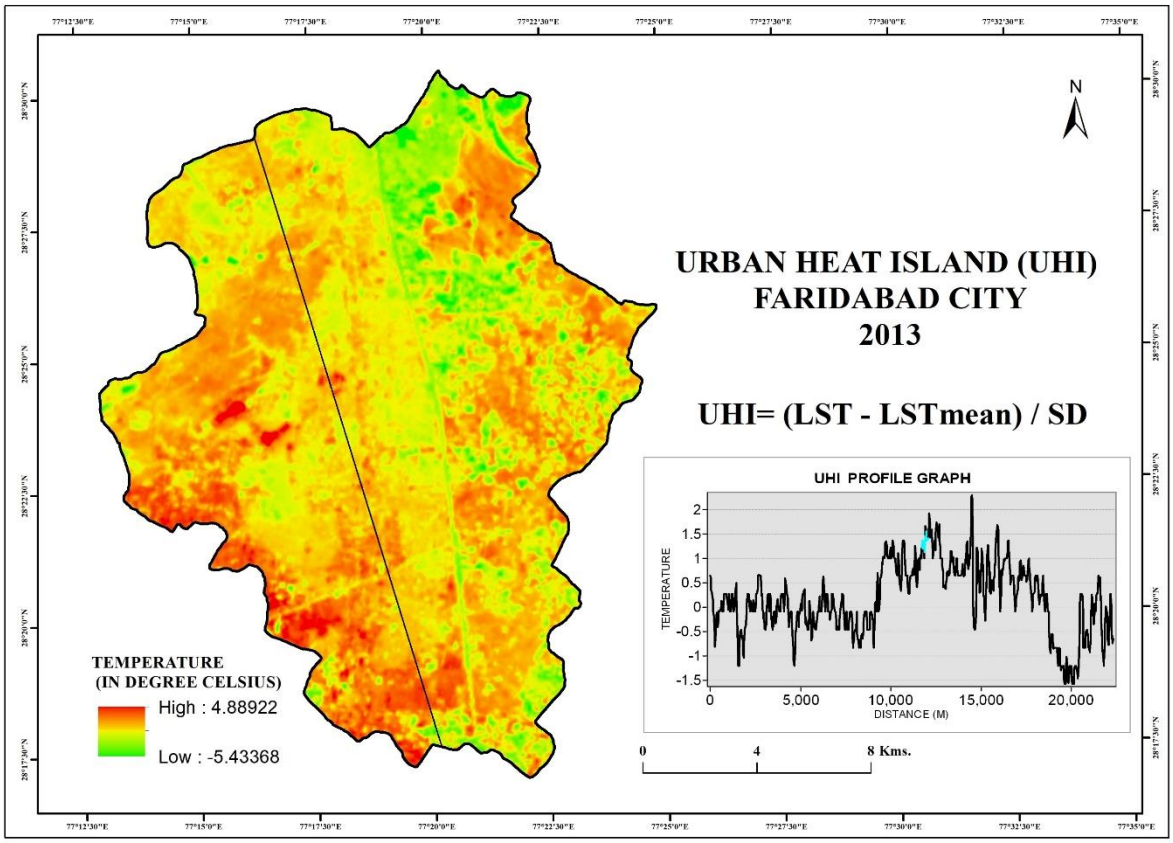

Fig 10 : Showing UHI map for year 2022

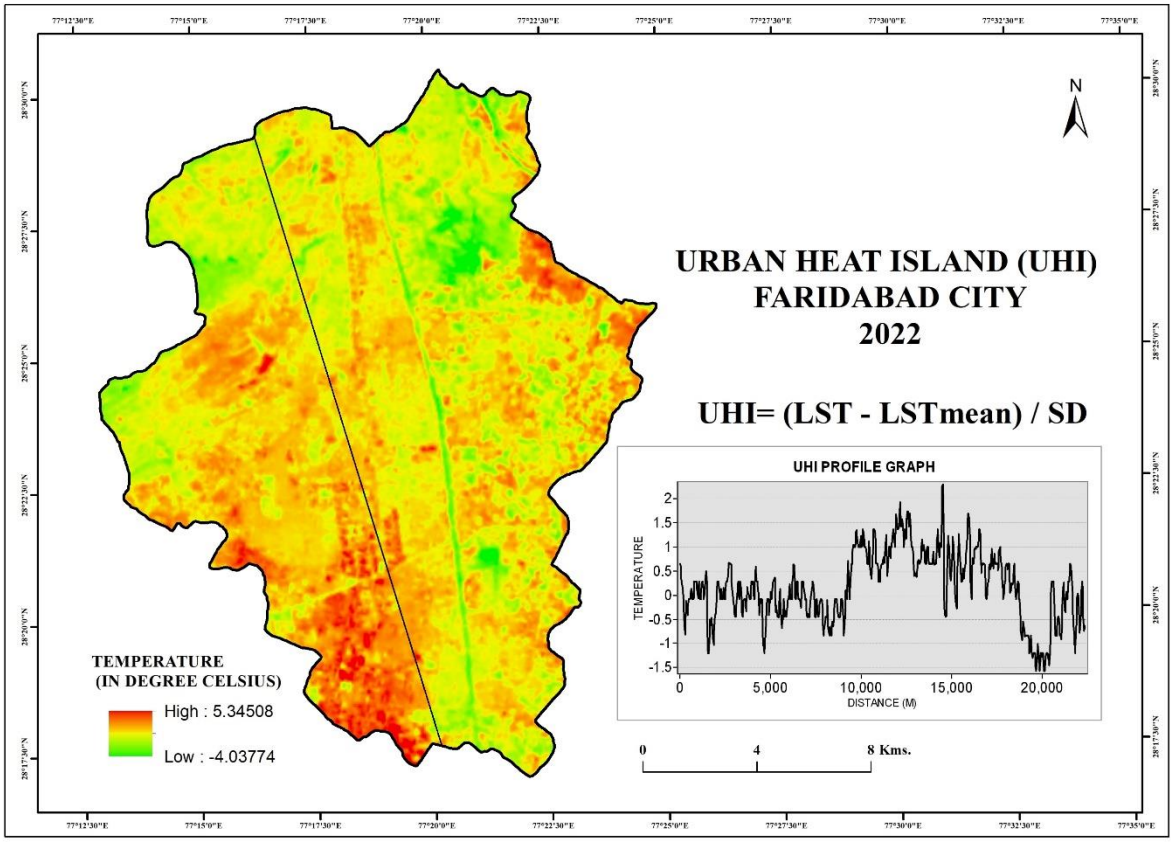

The effect of UHI also corresponds with the results of LST, showing maximum deviation over the Built-up and Barren land. Due to high heat retention capacity and low moisture, low evapotranspiration content over built-up and barren land the heat that traps forms UHI effect.

UTFVI

UTFVI is a commonly used index to more accurately reflect the surface urban heat island (SUHI) effect (Kafy et al., 2021a, Tomlinson et al., 2011). UTFVI concentrations are higher in the area and are significantly warmer than surrounding rural areas (Wang et al., 2017). Notable impacts of UTFVI include, but are not limited to, adverse effects on local air, humidity and air quality, reduced comfort and increased morbidity and non-economic diseases (Sejati et al., 2019).

Fig 11: Showing UTFVI map for year 2002, 2013, 2022

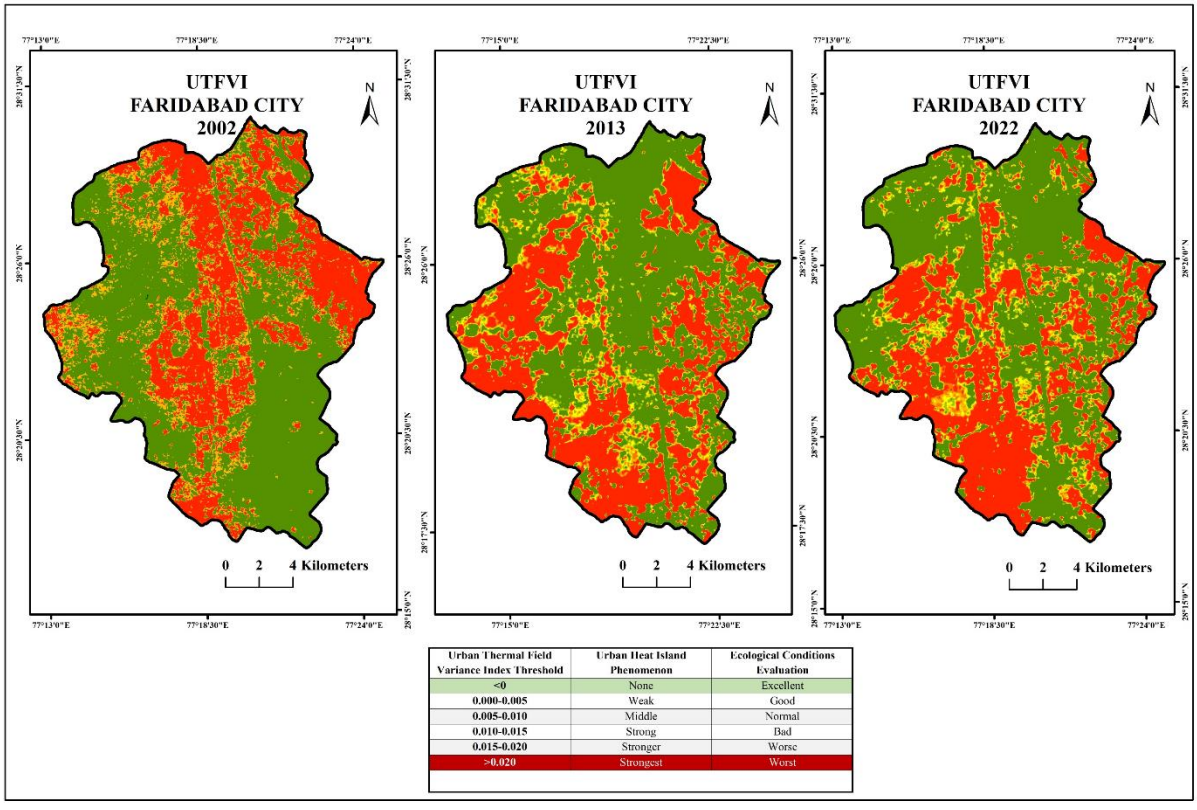

Urban Thermal Field Variance Index Threshold	Urban Heat Island Phenomenon	Ecological Conditions Evaluation
<0	None	Excellent
0.000-0.005	Weak	Good
0.005-0.010	Middle	Normal
0.010-0.015	Strong	Bad
0.015-0.020	Stronger	Worse
>0.020	Strongest	Worst

The results show the strongest effect of UTFVI can been seen over the Built-up area and with increase in the built-up area the area with strongest Urban heat island phenomenon increased. Built-up area also corresponds with the worst ecological condition. The area with none can be seen over the vegetation, agriculture and water body category with excellent ecological conditions.

Conclusion

In the present study, the effect on LST and UHI due to the increase in urbanization (built-up) was analysed in Faridabad city of India between years 2002, 2013 and 2022 using Landsat satellite images. The classified maps of Faridabad city were obtained for years 2002, 2013 and 2022 found that the area of 55.24 km2 of land cover was converted into built-up between years 2002 and 2022. Thus, a new index named UTFVI was proposed to quantify the urban heat intensity with increasing urbanization between years 2002, 2013 and 2022 in the Faridabad city. UTFVII value was found to increase in year which reveals that

urbanization has significant impact on urban temperatures. To study LST behavior based on LULC types, LST statistics were obtained for each land cover for four years: 2002, 2013, and 2022. As a result, the LST values of degraded and built-up land. The contribution to the UHI is a positive sign compared to the average LST of the entire region. Vegetation and water bodies were found to have low LST values compared to the average LST of the entire region, indicating a negative contribution to the UHI. In addition, the contribution of each land cover to the increase or decrease in LST was determined. Urbanization leads to two types of LULC changes: from barren to construction and from agriculture to construction. Mean differences in normalized LST for pixels converted from rural to urban from vegetation to urban from 2002 to 2022. Normalized LST decreased slightly from barren to urban pixels, but there was a significant decrease from vegetation to urban pixels. The established LST will increase. Therefore, the replacement of vegetation with urban soil increases the intensity of the impact of UHIs.
Therefore, this analysis discusses about quantification of the UHI effect with increasing urbanization and also the contribution of each land cover towards UHI.

References

1. Amir Siddique, Muhammad, Fan Boqing, and Liu Dongyun. "Modeling the Impact and Risk Assessment of Urbanization on Urban Heat Island and Thermal Comfort Level of Beijing City, China (2005–2020)." Sustainability 15, no. 7 (2023): 6043.
2. Aniello, C., Morgan, K., Busbey, A., & Newland, L. (1995). Mapping micro-urban heat islands using Landsat TM and a GIS. *Computers & Geosciences*, *21*(8), 965-969.
3. Arshad, S., Ahmad, S. R., Abbas, S., Asharf, A., Siddiqui, N. A., & ul Islam, Z. (2022). Quantifying the contribution of diminishing green spaces and urban sprawl to urban heat island effect in a rapidly urbanizing metropolitan city of Pakistan. *Land Use Policy*, *113*, 105874.
4. Kafy, A. A., Al Rakib, A., Akter, K. S., Rahaman, Z. A., Mallik, S., Nasher, N. R., ... & Ali, M. Y. (2021). Monitoring the effects of vegetation cover losses on land surface temperature dynamics using geospatial approach in Rajshahi City, Bangladesh. *Environmental Challenges*, *4*, 100187.
5. Kafy, A. A., Rahman, M. S., Hasan, M. M., & Islam, M. (2020). Modelling future land use land cover changes and their impacts on land surface temperatures in Rajshahi, Bangladesh. Remote Sensing Applications: Society and Environment, 18, 100314.
6. Kafy, A. A., Rahman, M. S., Hasan, M. M., & Islam, M. (2020). Modelling future land use land cover changes and their impacts on land surface temperatures in Rajshahi, Bangladesh. *Remote Sensing Applications: Society and Environment*, *18*, 100314.
7. Kafy, A. A., Shuvo, R. M., Naim, M. N. H., Sikdar, M. S., Chowdhury, R. R., Islam, M. A., ... & Kona, M. A. (2021). Remote sensing approach to simulate the land use/land cover and seasonal land surface temperature change using machine learning algorithms in a fastest-growing megacity of Bangladesh. *Remote Sensing Applications: Society and Environment*, *21*, 100463.
8. Li, N., Yang, J., Qiao, Z., Wang, Y., & Miao, S. (2021). Urban thermal characteristics of local climate zones and their mitigation measures across cities in different climate zones of China. *Remote Sensing*, *13*(8), 1468.
9. Liu, L., & Zhang, Y. (2011). Urban heat island analysis using the Landsat TM data and ASTER data: A case study in Hong Kong. *Remote sensing*, *3*(7), 1535-1552.
10. Luck, M., & Wu, J. (2002). A gradient analysis of urban landscape pattern: a case study from the Phoenix metropolitan region, Arizona, USA. Landscape ecology, 17, 327-339.

11. MacLachlan, A., Biggs, E., Roberts, G., & Boruff, B. (2021). Sustainable city planning: A data-driven approach for mitigating urban heat. *Frontiers in Built Environment*, *6*, 519599.
12. Maghrabi, A., Mohamed, M. F., Raman, S. N., Sulaiman, M. K. A. M., Yusoff, W. F. M., Abuhussain, M. A., & Almazroui, M. (2021). The Influence of Urbanism on the Urban Heat Island Phenomenon: Evidence from the KSA. *Journal of Hunan University Natural Sciences*, *48*(10).
13. Mathew, A., Khandelwal, S., & Kaul, N. (2018). Analysis of diurnal surface temperature variations for the assessment of surface urban heat island effect over Indian cities. *Energy and Buildings*, *159*, 271-295.
14. Prasad, S., & Singh, R. B. (2022). Urban Heat Island (UHI) Assessment Using the Satellite Data: A Case Study of Varanasi City, India. In *Smart Cities for Sustainable Development* (pp. 287-299). Singapore: Springer Nature Singapore.
15. Rahman, M. N., Rony, M. R. H., Jannat, F. A., Chandra Pal, S., Islam, M. S., Alam, E., & Islam, A. R. M. T. (2022). Impact of urbanization on urban heat island intensity in major districts of Bangladesh using remote sensing and geo-spatial tools. *Climate*, *10*(1), 3.
16. Sarrat, C., Lemonsu, A., Masson, V., & Guédalia, D. (2006). Impact of urban heat island on regional atmospheric pollution. *Atmospheric environment*, *40*(10), 1743-1758.
17. Sayad, B., Menni, Y., Imam, A. A., Fallatah, A., Faisal, K. S., Abed, A. M., ... & Hegazy, I. R. (2023). Diurnal characterization of the atmospheric urban heat island over urban hot agglomerations. International Journal of Low-Carbon Technologies, 18, 449-456.
18. Streutker, D. R. (2003). Satellite-measured growth of the urban heat island of Houston, Texas. *Remote sensing of Environment*, *85*(3), 282-289.
19. Swachh Survekshan - https://en.wikipedia.org/wiki/Swachh_Survekshan
20. Tafesse, B., & Suryabhagavan, K. V. (2019). Systematic modeling of impacts of land-use and land-cover changes on land surface temperature in Adama Zuria District, Ethiopia. *Modeling earth systems and environment*, *5*, 805-817.
21. Taha, H. (2008). Meso-urban meteorological and photochemical modeling of heat island mitigation. *Atmospheric Environment*, *42*(38), 8795-8809.
22. Tiangco, M., Lagmay, A. M. F., & Argete, J. (2008). ASTER-based study of the night-time urban heat island effect in Metro Manila. *International Journal of Remote Sensing*, *29*(10), 2799-2818.
23. Tran, H., Uchihama, D., Ochi, S., & Yasuoka, Y. (2006). Assessment with satellite data of the urban heat island effects in Asian mega cities. *International journal of applied Earth observation and Geoinformation*, *8*(1), 34-48.
24. Ullah, S., Ahmad, K., Sajjad, R. U., Abbasi, A. M., Nazeer, A., & Tahir, A. A. (2019). Analysis and simulation of land cover changes and their impacts on land surface temperature in a lower Himalayan region. *Journal of environmental management*, *245*, 348-357.
25. Ullah, S., Ahmad, K., Sajjad, R. U., Abbasi, A. M., Nazeer, A., & Tahir, A. A. (2019). Analysis and simulation of land cover changes and their impacts on land surface temperature in a lower Himalayan region. *Journal of environmental management*, *245*, 348-357.
26. Voogt, J. A., & Oke, T. R. (2003). Thermal remote sensing of urban climates. *Remote sensing of environment*, *86*(3), 370-384.
27. World Health Organization- https://www.who.int/
28. Zhang, J., & Wang, Y. (2008). Study of the relationships between the spatial extent of surface urban heat islands and urban characteristic factors based on Landsat ETM+ data. *Sensors*, *8*(11), 7453-7468.

29. Zhang, K., Wang, R., Shen, C., & Da, L. (2010). Temporal and spatial characteristics of the urban heat island during rapid urbanization in Shanghai, China. *Environmental monitoring and assessment*, *169*, 101-112.
30. Zhang, Y., Balzter, H., & Wu, X. (2013). Spatial–temporal patterns of urban anthropogenic heat discharge in Fuzhou, China, observed from sensible heat flux using Landsat TM/ETM+ data. *International journal of remote sensing*, *34*(4), 1459-1477.
31. Zhou, J., Chen, Y., Wang, J., & Zhan, W. (2010). Maximum nighttime urban heat island (UHI) intensity simulation by integrating remotely sensed data and meteorological observations. *IEEE Journal of Selected Topics in Applied Earth Observations and Remote Sensing*, *4*(1), 138-146.